Monthly Notices
of the
ROYAL ASTRONOMICAL SOCIETY

MNRAS **472,** 854–868 (2017)
Advance Access publication 2017 July 28

doi:10.1093/mnras/stx1891

A statistical spectropolarimetric study of Herbig Ae/Be stars

K. M. Ababakr,[1] R. D. Oudmaijer[1]★ and J. S. Vink[2]

[1]*School of Physics and Astronomy, University of Leeds, EC Stoner Building, Leeds LS2 9JT, UK*
[2]*Armagh Observatory, College Hill, Armagh BT61 9DG, UK*

Accepted 2017 July 24. Received 2017 July 20; in original form 2017 February 22

ABSTRACT

We present H α linear spectropolarimetry of a large sample of Herbig Ae/Be stars. Together with newly obtained data for 17 objects, the sample contains 56 objects, the largest such sample to date. A change in linear polarization across the H α line is detected in 42 (75 per cent) objects, which confirms the previous finding that the circumstellar environment around these stars on small spatial scales has an asymmetric structure, which is typically identified with a disc. A second outcome of this research is that we confirm that Herbig Ae stars are similar to T Tauri stars in displaying a line polarization effect, while depolarization is more common among Herbig Be stars. This finding had been suggested previously to indicate that Herbig Ae stars form in the same manner than T Tauri stars through magnetospheric accretion. It appears that the transition between these two differing polarization line effects occurs around the B7–B8 spectral type. This would in turn not only suggest that Herbig Ae stars accrete in a similar fashion as lower mass stars, but also that this accretion mechanism switches to a different type of accretion for Herbig Be stars. We report that the magnitude of the line effect caused by electron scattering close to the stars does not exceed 2 per cent. Only a very weak correlation is found between the magnitude of the line effect and the spectral type or the strength of the H α line. This indicates that the detection of a line effect only relies on the geometry of the line-forming region and the geometry of the scattering electrons.

Key words: techniques: polarimetric – circumstellar matter – stars: formation – stars: individual: Herbig Ae/Be – stars: pre-main-sequence.

1 INTRODUCTION

Herbig Ae/Be (HAeBe) stars, the more massive counterparts of T Tauri stars, are optically visible pre-main-sequence (PMS) stars with masses roughly between 2 and 10 $M_{\odot}$. This group of stars was first identified by Herbig (1960). With their intermediate masses, they play an essential role in addressing the formation of high-mass stars as they bridge the gap between low-mass stars, whose formation is fairly well understood and high-mass stars, whose formation still poses challenges. Lower mass stars are thought to form through magnetically controlled accretion (MA, e.g. Bouvier et al. (2007), whereas evidence for this mode of accretion is lacking for high-mass stars. Not only are higher mass stars not expected to be magnetic as their radiative envelopes would inhibit the presence of the magnetic fields that dominate the accretion in low-mass objects, these magnetic fields have also hardly been detected (e.g. Alecian et al. 2013). Traditionally, the change from MA and a different, hitherto unexplored, accretion mechanism was thought to be around the spectral type boundary M/K to F/A where the envelope structure changes from convective to fully radiative. However, it had long been known that Herbig Ae stars have different properties than Herbig Be stars and may form in a different manner (e.g. Fuente et al. 1998; Testi, Palla & Natta 1999; Ilee et al. 2014 who studied millimetre emission, clustering properties and CO first overtone emission properties, respectively). In addition, from various recent studies it appears that Herbig Ae stars are more similar to the T Tauri stars than to Herbig Be stars. For example, Grady et al. (2010) infer that the accretion shock regions in a Herbig Ae star are comparable in size and location to those in the magnetic lower mass objects. Schöller et al. (2016) interpret from the observed spectroscopic variability that a Herbig Ae star is currently undergoing magnetically controlled accretion in the same manner as the T Tauri stars. In contrast, dedicated modelling indicated that, if present at all, the magnetosphere in a Herbig Be star with spectral type B9IV must be small (Kurosawa et al. 2016). Indeed, Patel, Sigut & Landstreet (2017) find that magnetic fields are not required to explain the spectroscopic properties of early type Herbig Be stars.

★ E-mail: roud@ast.leeds.ac.uk

Finally, interferometric studies show that some of the hotter Herbig Be stars have much smaller near-infrared sizes than would be expected from the dust sublimation radius. This can be explained by optically thick gas in accretion discs reaching to the star (Kraus, Preibisch & Ohnaka 2008; Kraus 2015). A first indication that Herbig Ae stars share similarities with T Tauri stars but are different from Herbig Be objects emerged from a study into linear spectropolarimetry across Hα emission by Vink et al. (2002, 2003). Later, these authors found that the linear spectropolarimetric signatures observed around the Hα emission line in both T Tauri and Herbig Ae stars can be explained by compact Hα emission scattered off a circumstellar disc (Vink et al. 2005a, Vink, Harries & Drew 2005b; Mottram et al. 2007). This is suggestive of the notion that Herbig Ae stars may form in the same manner as T Tauri stars, where the compact Hα emission could arise from accretion hotspots or funnels due to magnetospheric accretion.

Further clues to this effect were presented by Cauley & Johns-Krull (2015) who found that the emission and absorption line properties of Herbig Be stars are significantly different from Herbig Ae stars, who in turn seem to have properties intermediate between Herbig Be and T Tauri stars. Finally, Fairlamb et al. (2015) found that the UV-excess of Herbig Ae stars can be explained by magnetospheric accretion, but that the earliest Herbig Be stars have too large UV-excesses to be explained by the usual accretion shock scenario (Muzerolle et al. 2004). For recent reviews on the subject of accretion in young stellar objects, including HAeBe stars, we refer the reader to Hartmann, Herczeg & Calvet (2016), Beltrán & de Wit (2016) and Oudmaijer (2017).

Linear spectropolarimetry is an effective technique to probe ionized inner circumstellar discs around stars on scales of order stellar radii, scales that are small enough to probe the accretion region of young stars. The technique was first successfully used to probe the circumstellar discs around classical Be stars (Clarke & McLean 1974; Poeckert & Marlborough 1976). These authors demonstrated that the continuum light is scattered and polarized by free electrons, while the hydrogen recombination line emission, which arises from a volume larger than where the electron scattering dominates, is not or hardly polarized. The use of the technique was extended by Oudmaijer & Drew (1999), Vink et al. (2002) and Mottram et al. (2007) to cover HAeBe stars. Vink et al. (2002) classified HAeBe stars according to their spectropolarimetric signature. In a study of 23 HAeBe objects, they found that many of the HBe stars (7 out of 12) show a depolarization line effect consistent with a circumstellar disc, similar to that observed in Be stars, while an intrinsic polarization line effect, as also observed in T Tauri stars is more dominant in most, 9 out of 11, less massive HAe stars. Their results suggest a physical switch from line polarization for HAe stars to depolarization in HBe stars.

To put these results on a firmer footing, a larger sample is needed to support and confirm the findings and draw statistical conclusions. In this work, we aim to provide a statistical investigation into the spectropolarimetric properties of HAeBe stars and their relation with their lower mass counterpart T Tauri stars. By collating all the data in the literature and adding newly obtained data, we present the spectropolarimetric results of a sample of 56 HAeBe objects, nearly three times larger than the sample of Vink et al. (2002). The paper is structured as follows. In Section 2, in order to properly interpret the data of this large sample, we start by an updated overview of the use of linear spectropolarimetry. This is followed by a discussion of the details of the sample selection, the complementary observations and the data reduction. In Section 3, we present the results which are discussed in Section 4. Finally, we conclude in Section 5.

2 METHODOLOGY, OBSERVATIONS AND DATA REDUCTION

2.1 Spectropolarimetry as a probe of inner regions

The technique of linear spectropolarimetry as applied here, exploits the fact that radiation will be scattered by free electrons in an ionized region. This results in the light to be polarized in the plane of the sky perpendicular to the original direction of travel. In case of a projected circular geometry of the scatterers on the sky – for example, a disc observed pole-on or a spherical distribution – all polarization vectors cancel, resulting in a net zero polarization. However, in case of an asymmetric distribution, a net polarization is observed. Most of the polarization due to free electrons is found to occur within a few stellar radii and results in polarizations of order 1–2 per cent (Cassinelli, Nordsieck & Murison 1987). We can take advantage of the fact that the stellar continuum photons and emission line photons originate from different locations and scatter differently off the free electrons, resulting in a different polarization across line and continuum. The spectropolarimetry around an emission line, most often Hα, has been observed, can therefore probe scales very close to the star. We note that many other scattering agents can give rise to polarization such as dust. However, whether circumstellar or interstellar, dust is located far away from the stellar and line emitting regions and it has a very broad wavelength dependence. As a consequence, the continuum and line radiation will be scattered in a similar fashion and no line effect is visible (e.g. Trammell, Dinerstein & Goodrich 1994).

Thus far, in the study of HAeBe stars, three types of 'line effect' can be identified and whereas the nature of the electron scattering process may be different, they share the fact that they probe the small scales of the electron scattering region. Let us start with the so-called depolarization effect. This had already been observed towards Be stars in the early seventies, and was in fact the first (indirect) proof that these stars are surrounded by small discs. The density of free electrons is the highest closest to the star, which is where the continuum photons emitted by the stellar photosphere will be polarized. In contrast, the hydrogen recombination line emission will be less polarized as it passes through a smaller ionized volume and hence encounters fewer free electrons. Therefore, a detection of a depolarization line effect across an emission line can immediately trace the presence of an ionized asymmetric structure with a size of order stellar radii. This is on much smaller scales than can be typically probed by the best imaging techniques (e.g. Kraus 2015; Mendigutía et al. 2015, 2017 on optical/near-infrared interferometry of HAeBe stars). Such a depolarization has been identified and confirmed to be due to a disc, as the polarization angles indicate that the scattering region is parallel to discs that have been observed at larger scales (e.g. Quirrenbach et al. 1997 for classical Be stars, and Wheelwright et al. 2011 for HAeBe stars, see reviews by Oudmaijer 2007 and Vink 2015). This depolarization line effect, similar to that observed in classical Be stars, follows the emission line and is more or less as broad as the emission. It can be detected in the polarization spectra, but also in the position angle spectra or both, depending on the (vector) contribution of the interstellar polarization. When translated into the Stokes *QU* parameters and plotted in the *(Q, U)* diagram, we will see a line excursion from the continuum towards the line (see Fig. 1, second column).

Alternatively, a different line effect signature can be detected when an emission line emerges from a compact, central, region and scatters off a circumstellar disc. This is usually accompanied by a flip in polarization or polarization angle (Vink et al. 2005b). When

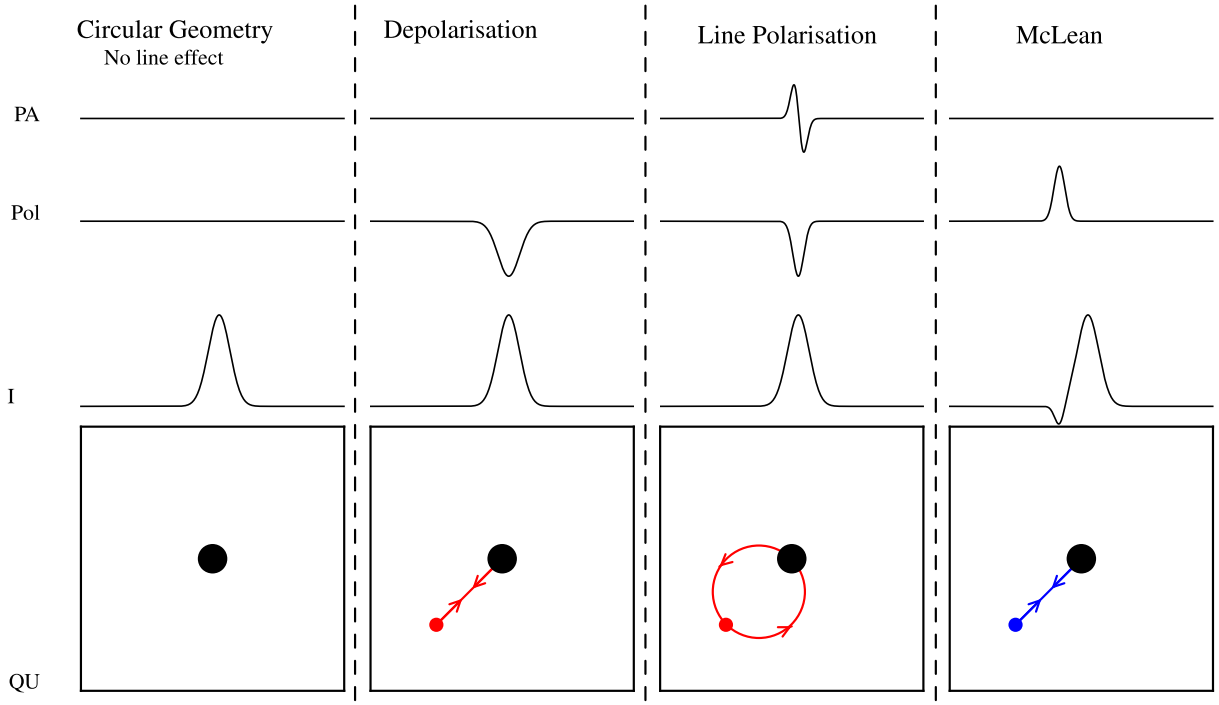

Figure 1. Schematic showing spectropolarimetry expectations across the H α line in triplots (top) and (*Q, U)* diagrams (bottom). In the triplot, the Stokes intensity (I) is shown in the bottom panel, polarization (per cent) in the centre, while the position angle (PA) is shown in the upper panel. The first column shows where the geometry of the circumstellar environment on the sky is circular and hence no line effect is detected. The other three columns show where the geometry on the sky is not circular and a line effect is seen. The second column shows a depolarization line effect, note that the depolarization across H α line is as broad as Stokes I. This depolarization line effect translates into (*Q, U)* diagram as a linear excursion from continuum knot towards the central line. The arrows in the (*Q, U)* diagrams indicate the polarization moves in and out of the line effect from blue to red wavelengths. Intrinsic line polarization is shown in third column, where H α line from the accretion compact region is scattered in a rotating disc. In this case, the polarization across H α is narrower that the width of Stokes I and a flip is seen in PA caused by a rotating disc. This flip is seen as a loop in (*Q, U)* diagram. Finally column 4 shows a different polarization signature across the absorption component of H α which is commonly known as the McLean effect. The figure is adapted from Vink et al. (2002).

mapped on the *(Q, U)* diagram, this particular line effect appears as a loop across the emission line (see Fig. 1, third column). The compact region is thought to be due to magnetospheric accretion, where the material from the disc is funnelled via accretion columns on to the stars, causing a shock on the photosphere. This type of line effect has been observed in T Tauri stars and HAe stars (Vink et al. 2005a). Importantly, the data provide the position angles of the discs in agreement with previous observations, while the models reproducing the line effect return disc sizes of order stellar radii, also in agreement with observations (Vink et al. 2005b; Vink 2015).

Thirdly, the absorption component of the emission line also produces a line effect signature that is commonly referred to as the McLean effect (McLean 1979). In this case, an enhanced polarization is detected across the absorption accompanying an emission line as direct, unscattered, light from the star is absorbed. This normally results in observing a typical (inverse) P Cygni line profile, depending on whether we consider infall of material or an outflow, respectively. The absorbed photons will be re-emitted isotropically and part of the emission will be scattered into our line of sight. If the distribution of the, inner, scattering material is not circular on the sky, an enhanced polarization will be detected across the absorption compared with the continuum light (see Fig. 1, fourth column).

Last but not least, if the geometry of the region containing the scatterers is circular on the sky, no line effect would be detected in most of the above cases (see Fig. 1, first column) since all polarization vectors will cancel. Such a circular geometry could be due to a spherical distribution of material or if the disc is viewed pole-on[1]

2.2 Construction of the sample

In order to perform a statistical study on the line polarimetry, a large sample of HAeBe stars is needed. We combined all our previous spectropolarimetric work across the H α line of HAeBe stars (Oudmaijer & Drew 1999; Vink et al. 2002, 2005a; Mottram et al. 2007; Wheelwright et al. 2011) into one sample. Our previous medium resolution linear spectropolarimetric data were obtained using the RGO spectrograph on the 3.9-m Anglo Australian Telescope (AAT; Oudmaijer & Drew 1999), the ISIS spectrograph on the 4.2-m on the William Herschel Telescope (WHT), La Palma (Oudmaijer & Drew 1999; Vink et al. 2002, 2005a; Mottram et al. 2007; Wheelwright et al. 2011; Ababakr, Oudmaijer & Vink 2016) and the FORS2 spectrograph mounted on ESO's 8.2-m Very Large Telescope (VLT) in Chile (Ababakr et al. 2016). These bring the total number of observed HAeBe objects to 56 (31 HBe and 25 HAe).

[1] A possible exception to this statement can occur in the case of the intrinsic line polarization. Emission emerging from an anisotropic source, such as an accretion hotspot, scattering off a circular geometry would also result in net polarization. However, we note that the position angles and size scales derived from our data are consistent with circumstellar discs in the case of the T Tauri stars.

Table 1. New HAeBe observations. Columns 1 and 2 show the target names, RA and Dec. are tabulated in columns 3 and 4. The *V*-band magnitude and spectral type are taken from Thé, de Winter & Pérez (1994) and SIMBAD, while for objects with new determinations of the photospheric temperature (Alecian et al. 2013; Fairlamb et al. 2015), the temperatures have been converted into a spectral type using Schmidt–Kaler's tables in Schaifers et al. (1982, Chapter 4). These are listed in columns 5 and 6. The integration times (column 8) denote the total exposures. Column 9 gives the SNR.

Name	Alt. name	RA (J2000)	Dec.(J2000)	*V*	Spec. type	Obs date	Exposure (s)	SNR
HD 163296	MWC 275	17:56:21.3	−21:57:21.9	6.9	A1	04-08-15	12 × 20	800
MWC 610	HD 174571	18:50:47.2	+08 42 10.1	8.9	B2	04-08-15	4 × 240	470
MWC 342	V1972 Cyg	20:23:03.6	+39 29 50.1	10.6	B(e)	04-08-15	24 × 20	275
HD 200775	MWC 361	21:01:36.9	+68:09:47.8	7.4	B3	04-08-15	24 × 15	860
HD 203024	BD+68 1195	21:16:03.0	+68:54:52.1	8.8	A1	04-08-15	4 × 240	480
V361 Cep	AS 475	21:42:50.2	+66:06:35.1	10.2	B3	04-08-15	8 × 300	660
HD 240010	MWC 655	22:38:31.8	+55:50:05.4	9.2	B1	04-08-15	4×240	545
V374 Cep	AS 505	23:05:07.6	+62:15:36.5	10.6	B0	04-08-15	8 × 300	400
MWC 863	HD 150193	16:40:17.9	−23:53:45.2	8.8	A2	05-08-15	12 × 150	780
V718 Sco	HD 145718	16:13:11.6	−22:29:06.7	8.9	A7	05-08-15	12 × 120	740
HD 141569	PDS 398	15:49:57.7	−03:55:16.3	7.1	A0	05-08-15	8 × 90	725
MWC 300	HBC 283	18:29:25.7	−06:04:37.3	11.6	B1	05-08-15	20 × 90	260
MWC 953	ALS 9906	18:43:28.4	−03:46:16.9	10.8	B2	05-08-15	12 × 180	370
MWC 623	V2028 Cyg	19:56:31.5	+31:06:20.1	10.9	B4(e)	05-08-15	24 × 45	90
V1977 Cyg	AS 442	20:47:37.5	+43:47:24.9	10.9	B8	05-08-15	12 × 300, 4× 45	475
MWC 1080	V628 Cas	23:17:25.6	+60:50:43.4	11.6	B0	05-08-15	20 × 300	440
HD 144432	PDS 78	16:06:57.9	−27:43:09.8	8.2	A8I	05-08-15	12 × 150	680

These objects are presented in Table 2. A sample of 29 HAeBe stars, of which 19 objects are in common with our sample, was observed spectropolarimetrically by Harrington & Kuhn (2009) but due to technical issues, these authors did not have information on the polarization angle, and we decided not to include the remaining 10 objects for the analysis.

Our sample is the largest (linear) spectropolarimetric survey of HAeBe stars that has been published to date. The vast majority, 52, of the objects were selected from the HAeBe catalogue of Thé et al. (1994), 10 of which are in other tables (extreme emission lines, other early emission line stars and non-emission line early type stars) in Thé et al. (1994). We proceed under the assumption that they are young stars. The remaining five objects were taken from the HAeBe candidate stars of Vieira et al. (2003). The final sample covers nearly 50 per cent of the HAeBe catalogue, where the majority was chosen from the Northern hemisphere. Most of the remaining targets in the catalogue are too faint ($V \geq 13.5$) and would require very long exposure times as the spectropolarimetry needs high SNR. The combined Hα spectropolarimetric observations allow us to conduct the most powerful statistical investigation into the nature of linear polarization in the circumstellar environment of HAeBe stars. To compare the spectropolarimetric results of HAeBe stars and their lower mass counterparts T Tauri stars, the spectropolarimetric results of a sample of 9 T Tauri stars are taken from Vink et al. (2005a).

2.3 Complementary observations

Seventeen targets were selected from the HAeBe catalogue of Thé et al. (1994) and candidates of Vieira et al. (2003) to complement previous spectropolarimetric results. The list of objects and the log of the observations are presented in Table 1. The SNR is measured over a range of 10 Å around 6700 Å where the continuum is the flattest and the spectral lines are absent.

The new linear spectropolarimetric data were obtained with the ISIS spectrograph on the WHT, La Palma, during the nights of 2015 August 4 and 5. The log of the observations is provided in Table 1. The 1200R grating centred at 6800 Å, with a spectral range of 1000 Å, was employed with a windowed 351 × 4200 pixel CCD and a slit width of 1.0 arcsec. This setup provides a spectral resolution of ∼35 km s^{-1} as measured from arc lines around the Hα line. The seeing was less than 1.0 arcsec throughout both nights. The polarization optics, which consist of a rotating half-wave plate and a calcite block, were used in order to perform linear polarization observations. The calcite block separates the light into two perpendicularly polarized light beams, the ordinary (O) and extraordinary (E) beam. One complete set of observations consists of four exposures with the half-wave plate set at angles: 10°, 55°, 32.°5 and 77.°5. The dekker with 18 arcsec slot separation was used to observe the object and the sky simultaneously. Several cycles of observations per object were obtained at the four position angles to check for the consistency of the results. Several short exposures were taken for objects with strong Hα line to avoid saturation. Polarized standard stars and zero-polarized standard stars were observed each night to calibrate for the instrumental polarization and angle offset.

The data reduction was carried out using IRAF (Tody 1993), which includes bias subtraction, flat-fielding, sky subtraction and extraction of the O and E spectra. The extracted spectra were imported into the TSP package (Bailey 1997) to compute the Stokes parameters. The wavelength calibration was performed using FIGARO. For analysis purposes, the data were imported into the POLMAP package (Harries 1996). Multiple observations of the same targets provided very consistent results. As the observations were obtained at the parallactic angle to achieve high SNR, the angle calibration was performed using the observed polarized standard stars. The instrumental polarization is found to be ∼0.1 per cent while the angle offset is found to be less than 0.°5 from the observation of unpolarized and polarized standard stars. As the instrumental and interstellar polarization add a wavelength independent vector to the observed spectra, we did not correct the observed polarization for them.

3 RESULTS

We begin with a brief presentation of the new data, before we focus on the statistical results of the full sample of spectropolarimetric data on HAeBe stars.

MNRAS 472, 854–868 (2017)

Table 2. The Hα spectropolarimetric results of the largest sample of HAeBe stars. The measurements are taken in the *R* band. Columns 5 and 6 list the Stokes (I) characteristics EW and line to continuum ratio, the error in both are typically less than 5 per cent. Columns 7–12 list line spectropolarimetric characteristics of each targets. Column 7 shows whether there is a line effect across the Hα line or not and the magnitude of the line effect is presented in column 8. The typical error is 10 per cent. $\Delta\lambda(pol)$ and the fractional width $\Delta\lambda(pol)/\Delta\lambda(I)$ are listed in columns 9 and 10, $\Delta\lambda(pol)$ and $\Delta\lambda(pol)$ are measured at full width at zero intensity (FWZI). $\Delta\lambda(pol)$ is the width over which the polarization changes across the line, column 11 lists whether there is a flip in polarization or polarization angle or not across the line. The classification of the line effect is presented in column 12. The continuum polarization and polarization angle are listed in columns 13 and 14 and the intrinsic polarization angle is listed in column 15.

No.	Object	Obs date	Spec. type	Hα EW (Å)	Line/cont.	Line effect	Mag. (per cent)	$\Delta\lambda(pol)$ (Å)	$\frac{\Delta\lambda(pol)}{\Delta\lambda(I)}$	Flip	Class.	$P_{\rm cont}$(per cent)	$\theta^{\circ}_{\rm cont}$	$\theta^{\circ}_{\rm intr}$	Ref.
1	HD 163296	04-08-15	A1	− 16.4	3.9	Y	0.51	15.0	0.86	Y	P	0.162 ± 0.005	48.88 ± 0.90	144 ± 10	1
		01-04-12		− 14.9	3.8	Y		19.5	1.05	Y	P	0.70 ± 0.01	1.60 ± 0.20	112 ± 10	2
2	MWC 610	04-08-15	B2	2.0	1.01	N	–	–	–	–	–	2.507 ± 0.006	81.86 ± 0.07	–	1
3	MWC 342	04-08-15	B(e)	− 264.5	54.0	Y	0.75	17.5	0.71	N	D	0.736 ± 0.016	102.17 ± 0.57	180 ± 5	1
4	HD 200775	04-08-15	B3	− 75.0	10.5	Y	0.40	29.0	1.10	N	D/M	0.782 ± 0.005	93.46 ± 0.19	88 ± 5	1
		18-12-99		− 63.0	8.5	Y	0.50	45.0	1.13	N	D/M	0.81 ± 0.01	96 ± 1	93 ± 2	3, 6
		13-12-03		− 47.0	8.2	Y	0.35	–	–	N	D/M	0.801 ± 0.003	93.6 ± 0.1	90	4
5	HD 203024	04-08-15	A1	7.6	0.6	N	–	–	–	–	–	0.496 ± 0.007	49.23 ± 0.42	–	1
6	V361 Cep	04-08-15	B3	− 32.5	5.9	N	–	–	–	–	–	0.846 ± 0.007	87.84 ± 0.25	–	1
7	HD 240010	04-08-15	B1	− 14.3	2.4	Y	0.40	27.0	0.87	N	D	3.018 ± 0.008	73.12 ± 0.08	100 ± 5	1
8	V374 Cep	04-08-15	B0	− 33.6	5.2	Y	1.30	27.5	0.81	N	D	4.841 ± 0.008	128.46 ± 0.05	169 ± 5	1
9	MWC 863	05-08-15	A2	− 1.6	3.0	Y	0.80	15.0	1.00	N	M/P	5.319 ± 0.004	57.25 ± 0.02	55 ± 5	1
10	V718 Sco	05-08-15	A7	6.3	1.1	Y	0.50	12.0	0.72	N	M	0.457 ± 0.007	83.07 ± 0.44	–	1
11	HD 141569	05-08-15	A0	4.2	1.3	N	–	–	–	–	–	0.639 ± 0.004	86.91 ± 0.18	–	1
		27-12-01		− 5.5	1.4	N	–	–	–	–	–	0.647 ± 0.005	85.2 ± 0.2	–	1
12	MWC 300	05-08-15	B1	− 128.0	71.0	Y	0.73	3.5	0.29	N	M	4.467 ± 0.016	57.58 ± 0.10	–	1
13	MWC 953	05-08-15	B2	− 34.1	12.8	N	–	-	–	–	–	2.555 ± 0.008	75.60 ± 0.10	–	1
14	MWC 623	05-08-15	B4(e)	− 119.3	38.0	N	–	–	–	–	–	2.548 ± 0.011	53.50 ± 0.12	–	1
15	V1977 Cyg	05-08-15	B8	− 31.2	6.5	Y	1.20	5.8	0.34	N	M	2.774 ± 0.008	168.89 ± 0.08	–	1
16	MWC 1080	18-12-99	B0	− 101.0	18.0	Y	0.40	50.0	1.11	N	D	1.73 ± 0.01	77 ± 1		3
		05-08-15		− 126.0	19.0	Y	0.30	7.8	0.29	N	M	1.601 ± 0.007	82.24 ± 0.12	–	1
		29-09-04		− 100.0	30.0	Y	0.30	–	–	N	D	1.51 ± 0.01	77.2 ± 0.1	–	6
		09-11-08		–	–	–	–	–	–	–	–	1.7 ± 0.1	78 ± 1	–	7
17	HD 144432	05-08-15	A8	− 2.5	2.5	Y	0.81	12.5	1.00	N	D/M	0.432 ± 0.004	12.92 ± 0.25	175 ± 10	1
18	PDS 27	04-02-12	B3	− 120.8	18.0	Y	1.00	18.0	0.57	N	M	8.80 ± 0.01	18.40 ± 0.04	77 ± 10	2
19	PDS 37	05-02-12	B3	− 122.6	19.4	Y	1.60	15.5	0.55	N	M	5.20 ± 0.01	130.00 ± 0.06	56 ± 10	2
20	PDS 133	21-01-12	B6	− 94.5	20.7	Y	2.00	6.0	0.28	N	M	2.30 ± 0.04	37.70 ± 0.50	126 ± 10	2
21	HD 98922	16-01-12	B9	− 17.9	6.0	Y	0.80	9.8	0.72	N	D/M	0.40 ± 0.01	174.90 ± 0.30	22 ± 10	2
22	GU CMa	07-01-12	B2	− 11.1	2.6	Y	0.95	12.8	0.70	N	D	1.60 ± 0.01	14.60 ± 0.01	127 ± 10	2
		11-01-95		− 14.0	3.0	N	–	–	–	–	–	1.15 ± 0.01	19 ± 1	–	5
		08-11-08		–	2.3	Y	0.30	–	–	N	D	0.8 ± 0.1	24 ± 1	–	7
		10-12-03		− 9.3	2.2	N	–	–	–	–	–	1.726 ± 0.006	27.0 ± 0.1	–	4
23	CPD-485215	20-01-12	B6	− 100.8	19.6	Y	0.86	17.0	1.00	N	D	1.70 ± 0.01	9.50 ± 0.20	62 ± 10	2
24	HD 85567	30-12-11	B7	− 43.5	9.9	Y	0.50	17.0	0.87	N	D	0.38 ± 0.01	133.90 ± 0.60	31 ± 10	2
		30-03-12		− 42.1	10.2	Y?	–	–	–	–	–	0.26 ± 0.02	134.50 ± 2.10	–	2
25	V380 Ori	03-01-12	A0	− 71.1	13.6	Y	1.10	7.0	0.54	N	P	0.70 ± 0.01	98.40 ± 0.06	10 ± 10	2
		12-10-11		− 82.7	15.5	N	–	–	–	–	–	0.70 ± 0.01	95.15 ± 1.00	–	2
		31-12-96		− 79.0	14.0	N	–	–	–	–	–	1.26 ± 0.01	96 ± 1	–	5
26	HD 104237	16-01-12	A7	− 27.2	6.5	Y?	–	–	–	–	Complex	0.35 ± 0.01	174.60 ± 0.60	–	2
27	BF Ori	12-10-11	A2	1.0	1.9	Y?	–	–	–	–	Complex	0.70 ± 0.01	44.00 ± 0.06	–	2
		09-11-08		–	1.8	N	–	–	–	–	–	0.6 ± 0.1	58 ± 1	–	7
28	MWC 137	20-12-99	B0	− 404.0	70.0	Y	0.85	55.0	0.92	N	D	6.07 ± 0.01	160 ± 1	25 ± 10	3
		31-12-96		− 550.0	83.0	Y	0.69	28.6	1.06	N	D	6.11 ± 0.01	162 ± 1	30 ± 5	5
29	BD+40 4124	19-12-99	B2	− 113.0	17.0	Y	1.26	30.0	0.75	N	D	1.21 ± 0.01	8 ± 1	83 ± 8	3
30	MWC 147	18-12-99	B6	− 60.0	13.0	Y	0.60	18.0	0.50	–	Complex	1.05 ± 0.01	100 ± 1	–	3

Table 2 – *continued.*

No.	Object	Obs date	Spec. type	Hα EW (Å)	Line/cont.	Line effect	Mag. (per cent)	$\Delta\lambda(pol)$ (Å)	$\frac{\Delta\lambda(pol)}{\Delta\lambda(I)}$	Flip	Class.	$P_{\rm cont}$ (per cent)	$\theta^{\circ}_{\rm cont}$	$\theta^{\circ}_{\rm intr}$	Ref.
		30-12-96		− 63.0	11.0	Y	0.25	6.8	0.33	N	–	1.06 ± 0.01	102 ± 1	–	5
		09-11-08		–	–	Y	–	–	–	N	–	1.0 ± 0.1	100 ± 1	–	7
31	HD 58647	19-12-99	B9	− 8.6	2.4	Y	1.20	10.0	0.67	N	Complex	0.14 ± 0.01	127 ± 1	–	3
32	MWC 120	19-12-99	B9	− 29.0	6.3	Y	1.28	13.0	0.65	N	P	0.35 ± 0.01	76 ± 1	–	3
		11-01-95		− 17.0	4.9	Y	–	–	–	N	–	0.29 ± 0.01	121 ± 1	–	5
		29-09-04		− 20.0	–	Y	–	–	–		–	0.40 ± 0.01	115.4 ± 0.2		6
33	MWC 789	19-12-99	B9	− 46.0	10.0	Y	0.70	21.0	0.95	Y	Complex	0.92 ± 0.01	174 ± 1	178 ± 10	3
34	AB Aur	18-12-99	A0	− 40.0	8.0	Y	1.30	17.0	1.00	N	Complex	0.11 ± 0.01	54 ± 1	160 ± 5	3
35	XY Per	20-12-99	A2	− 6.7	2.3	Y	0.60	15.0	0.88	Y	P	1.60 ± 0.01	132 ± 1	–	3
		10-11-08		–	–	N	–	–	–	–	–	1.4 ± 0.1	128 ± 1	–	7
36	MWC 480	19-12-99	A5	− 21.0	4.8	Y	2.15	12.0	0.67	Y	P	0.38 ± 0.01	52 ± 1	–	3
		30-09-04		− 11.0	–	Y	–	–	–	–	P	0.20 ± 0.01	64.9 ± 1.3	–	6
		26-12-01		− 20.5	4.9	Y	–	–	–	–	M	0.176 ± 0.005	63.0 ± 0.8	55	4
37	HD 244604	19-12-99	A2	− 14.0	4.5	Y	0.32	10.0	0.56	Y	P	0.44 ± 0.01	119 ± 1	–	3
38	T Ori	20-12-99	A2	− 12.0	3.9	Y	2.20	5.0	0.26	N	P	0.39 ± 0.01	97 ± 1	–	3
39	HD 245185	20-12-99	A0	− 17.0	3.7	Y	1.14	10.0	0.56	Y	P	0.2 ± 0.011	168 ± 1	–	3
40	IL Cep	08-11-08	B3	− 20.0	3.5	N	–	–	–	–	–	4.24 ± 0.01	102 ± 1	–	3
		19-12-99		–	–	N	–	–	–	–	–	4.3 ± 0.01	100 ± 1	–	7
41	MWC 758	19-12-99	A7	− 17.0	4.0	N	–	–	–	–	–	0.07 ± 0.01	179 ± 1	–	3
		08-11-08		–	–	N	–	–	–	–	–	0.5 ± 0.1	47 ± 1	–	7
42	HD 35929	19-12-99	F2	− 3.2	2.0	N	–	–	–	–	–	0.12 ± 0.01	51 ± 1	–	3
43	SV Cep	12-12-03	A0	− 11.0	2.0	Y	0.86	20.0	1.00	Y	P	1.293 ± 0.011	67.6 ± 0.2	–	4
44	CQ Tau	20-12-99	F2	− 2.7	1.6	Y	0.80	3.0	0.17	N	P	0.27 ± 0.01	83 ± 1	–	3
45	MWC 158	01-01-97	B6	− 58.0	13.0	Y	0.64	15.75	0.94	N	D	0.65 ± 0.01	154 ± 1	155 ± 5	5
46	HD 87643	01-01-97	B3	− 196.0	26.0	Y	1.15	31.0	0.97	N	D	0.75 ± 0.01	164 ± 1	–	5
		31-12-96		− 186.0	25.0	Y	1.27	29.3	0.96	N	D	0.84 ± 0.01	168 ± 1	–	5
47	W Ori	11-01-95	B3	− 3.5	1.6	N	–	–	–	–	–	0.27 ± 0.01	55.7 ± 0.6	–	5, 6
48	MWC 166	30-12-96	B0	− 14.0	2.6	Y	0.20	24.4	1.01	N	D	0.49 ± 0.01	44.9 ± 0.1	136 ± 4	5, 6
		18-12-99		− 2.8	1.6	N	–	–	–	–	–	0.20 ± 0.01	34 ± 1	–	3
		11-12-03		0.59	0.75	N	–	–	–	–	–	0.164 ± 0.003	36.8 ± 0.4	–	4
49	HD 179218	08-11-08	A0	–	2.1	Y	0.50	8.0	0.57	N	P	0.5 ± 0.1	111 ± 1	∼45	7
50	HK Ori	08-11-08	A3	–	6.0	Y	1.00	15.0	0.90	N	D	1.4 ± 0.1	113 ± 1	169 ± 6	7
51	V586 Ori	09-11-08	A0	–	3.9	Y	0.60	13.0	1.00	N	D	0.9 ± 0.1	84 ± 1	81 ± 8	7
52	MWC 297	15-07-98	B1	− 520.0	100.0	N	–	–	–	–	–	1.90 ± 0.01	86 ± 1	–	5
53	HD 76534	11-01-95	B3	− 7.5	2.0	N	–	–	–	–	–	0.52 ± 0.01	124 ± 1	–	5
54	AS 116	01-01-97	B5	− 90.0	18.0	N	–	–	–	–	–	1.41 ± 0.01	30 ± 1	–	5
55	Hen 3-230	30-12-96	Be	− 315.0	64.0	N	–	–	–	–	–	1.61 ± 0.02	30 ± 1	–	5
56	HD 45677	11-01-95	B3	− 200.0	35.0	Y	–	–	–	–	–	0.33 ± 0.01	11 ± 1	–	5
		30-12-96		− 200	34	Y	–	–	–	–	–	0.14 ± 0.02	143 ± 3	–	5
57	R Mon	12-10-11	B8	− 98.6	12.6	Y	4.60	30.5	1.00	–	–	8.10 ± 0.02	69.40 ± 0.07	–	2
		01-02-12		− 105.5	12.9	Y	9.30	26.5	0.82	–	–	12.15 ± 0.01	67.70 ± 0.04	–	2
58	LKHα 218	31-12-96	B9	− 20.0	6.0	N	–	–	–	–	–	1.91 ± 0.02	19 ± 1	–	5
59	AS 477	19-12-99	A0	− 19.0	4.4	N	–	–	–	–	–	0.43 ± 0.01	56 ± 1	–	3
60	KMS 27	19-12-99	A0	− 7.2	2.5	Y	–	–	–	–	–	0.13 ± 0.01	52 ± 1	–	3

Notes. D: depolarization, P: polarization, M: McLean.

References. (1) This work; (2) Ababakr et al. (2016); (3) Vink et al. (2002); (4) Vink et al. (2005a); (5) Oudmaijer & Drew (1999); (6) Mottram et al. (2007); (7) Wheelwright et al. (2011).

R Mon was discarded as the large magnitude of the line effect (∼10 per cent) was not caused by electron scattering.

LKHα, AS 477 and KMS 27 were discarded as they suffered from too low photon counts.

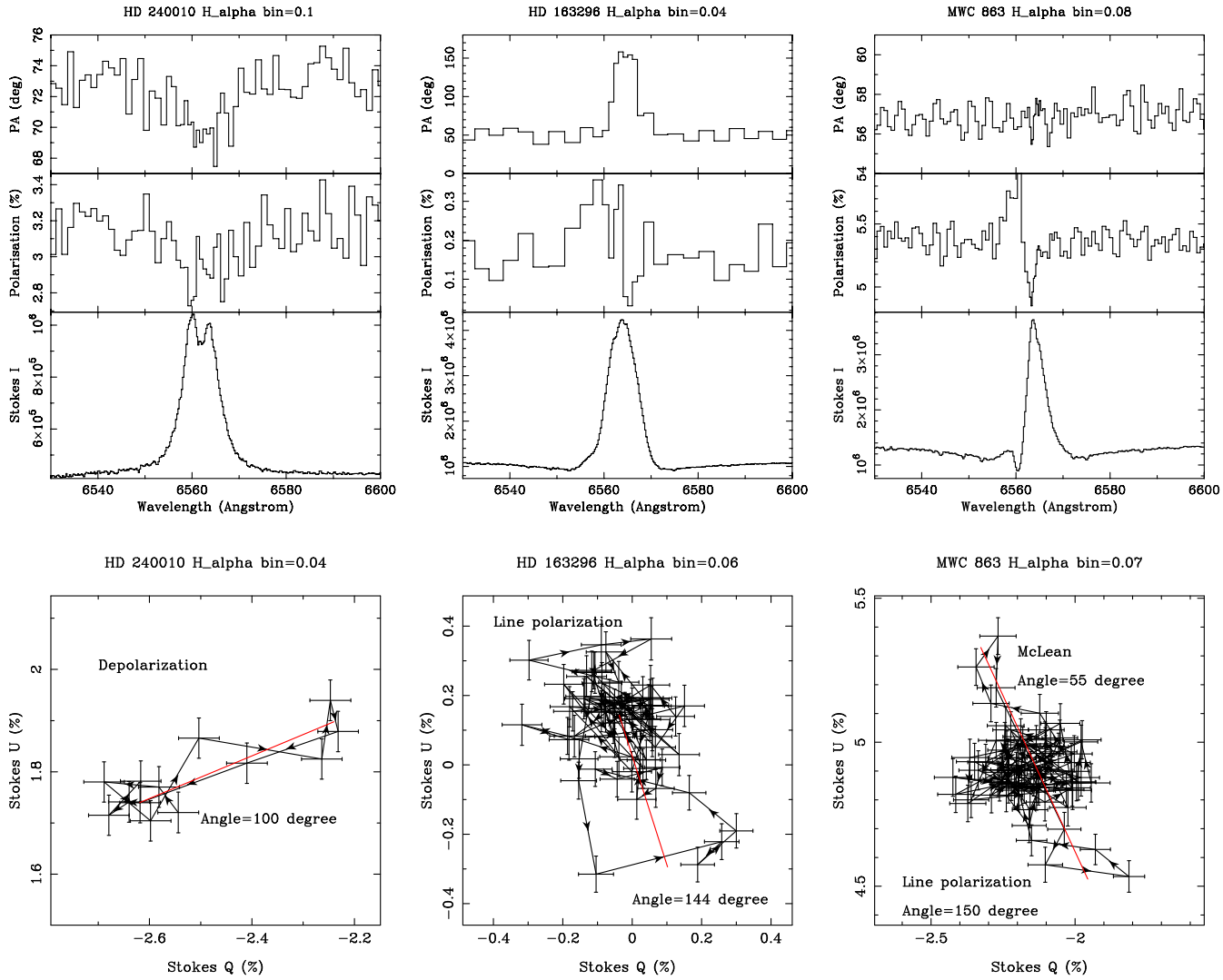

Figure 2. Examples of the various line effects in the Hα spectropolarimetry of three objects for which new data were obtained. The data are presented as a combination of triplots (top) and (*Q, U)* diagrams (bottom). In the triplot polarization spectra, the Stokes intensity (I) is shown in the bottom panel, polarization (per cent) in the centre, while the position angle (PA) is shown in the upper panel. The *Q* and *U* Stokes parameters are plotted against each other below each triplot. The data are rebinned to a constant error in polarization, which is indicated at the top of each plot. The arrows in the (*Q, U)* diagrams indicate the polarization moves in and out of the line effect from blue to red wavelengths. The solid line in the (*Q, U)* diagrams represents the direction of the intrinsic polarization angle.

3.1 Hα spectropolarimetry-new observations

In the new observations, 11 objects out of 17 had never been observed with linear spectropolarimetry. Hα spectropolarimetry was performed for all the targets in Table 1 and the results of the entire sample are presented in Table 2 and in Appendix A (Fig. A1). In total, 11 objects show a possible line effect across the Hα line.

The spectropolarimetric results of three objects from these new observations, selected as they exhibit the three different line effect signatures, are shown in triplots in the upper half of Fig. 2. In this triplot, the Stokes I (normal intensity) is shown in the lower panel, the polarization percentage in the middle, while the position angle (PA) is displayed in the upper panel. The results are also represented in a Stokes (*Q, U)* diagram (bottom) in Fig. 2 using the same wavelength range of the triplot spectra, but sometimes with a different binning. HD 240010 shows a broad depolarization line effect across the Hα line in both polarization and polarization angle spectra. The line effect is as broad as the emission line and it appears as a linear excursion in the (*Q, U)* diagram, the contribution of interstellar polarization has likely introduced a signature in the position angle, but will have only added a constant value in the *(Q,U)* diagram, which still shows a straight line. An intrinsic polarization line effect is seen across the Hα line in HD 163296, the effect is narrower than the depolarization line effect and there is a flip in polarization across the line. This flip appears as a loop when it is mapped on the (*Q, U)* diagram. MWC 863 shows two different line effects, a McLean line effect is seen across the absorptive component while the emission line displays a narrow polarization which is identified with intrinsic polarization (in the following sections, the classification criteria are outlined). Fig. 2 also shows the intrinsic polarization angle which is measured from the slope of the line effect in the (*Q, U)* diagram. For the depolarization line effect, the angle is measured from the (unpolarized) line to the (polarized) continuum while for the intrinsic polarization and McLean effect it is measured from continuum to (polarized) line (see the discussion in Ababakr

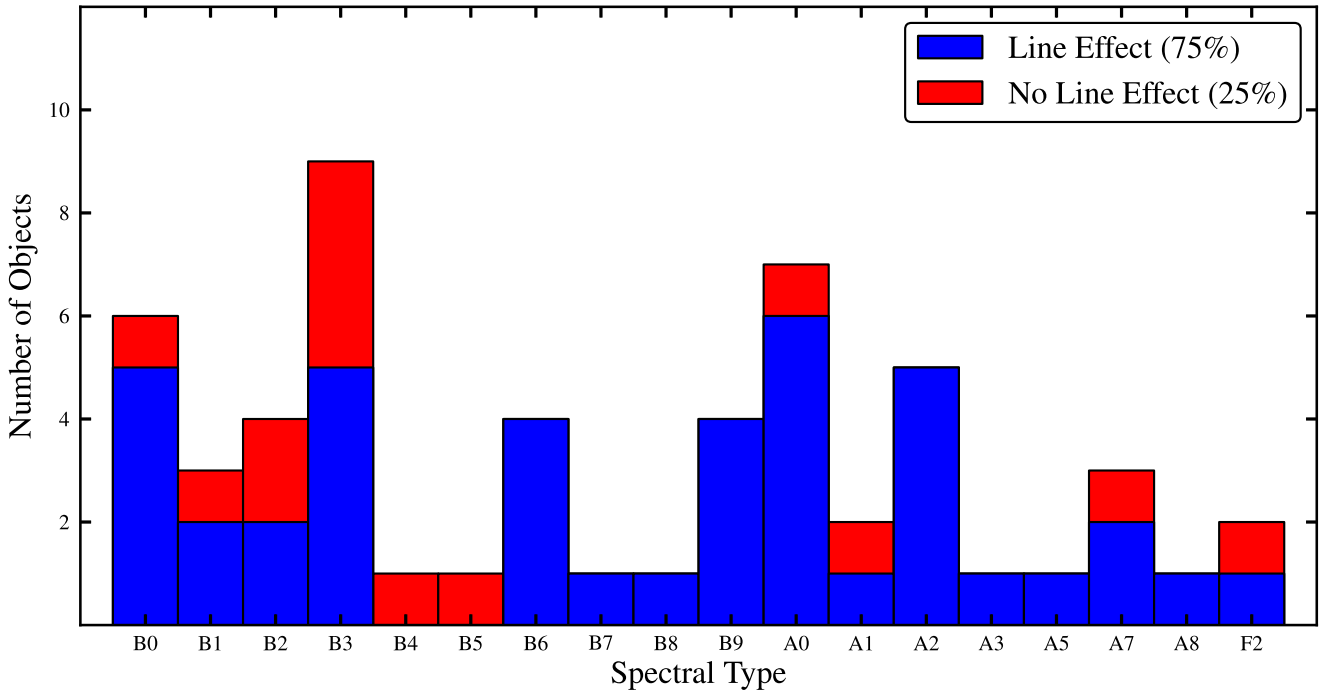

Figure 3. The figure shows the observed line effect across the Hα line in each subgroup of spectral type of the whole sample of HAeBe stars that have been observed spectropolarimetrically. Please note that spectral types such as A4, A6 and A9 are not always defined in spectral type classification schemes, and will thus be missing in a graph such as this (Jaschek & Jaschek 1990).

et al. 2016). Although the direction for both the depolarization (HD 240010) and intrinsic polarization (HD 163296) are the same in the respective *QU* graphs, the intrinsic polarization angles differ, as this angle is measured from the line centre to the continuum in the case of the depolarization, it is measured in the opposite direction for the intrinsic polarization.

3.2 Statistical results

We present here Hα spectropolarimetric results from a sample of 56 HAeBe stars combined from this work and the literature. We begin with discussing the observed line effect and its type, before we focus on the magnitude and width of the line effect.

The Hα spectropolarimetric results of each target are listed in Table 2. Columns 3 and 6 list the spectroscopic characterization of Stokes I, the intensity spectrum. The line polarimetric properties of each target are tabulated in columns 7–12 and 15. Finally, the continuum spectropolarimetric measurements are listed in columns 13 and 14. As can be seen in Fig. 3 and Table 2, a line effect is detected across Hα in 42/56 objects (75 $\pm$ 6 per cent, errors reflecting the 1σ confidence interval of a sample proportion), divided equally between 21 HBe and 21 HAe stars. Fourteen objects (25 $\pm$ 6 per cent) do not show any signs of a line effect. The detection rate for Herbig stars of spectral type B0–B7 is 66 $\pm$ 9 per cent while that of the later type (i.e. all other) objects is 85 $\pm$ 7 per cent, a difference that is close to 3σ.

3.2.1 Line effect signatures

The decision on whether to classify a line effect as depolarization or intrinsic polarization can sometimes be subjective. To avoid such biases, we aim to differentiate between the depolarization and the line polarization effect in a quantitative manner. To this end, the width of the line effect can be used as proxy (see Table 2). The method was first used by Vink et al. (2002, 2005a) to categorize the line effects. They statistically classified stars according to the fractional width [$\Delta\lambda(pol)/\Delta\lambda(I)$] at which the polarization changes across the line. This quantity measures the width of the polarization over the line divided by the width of the line itself. Generally a wide fractional width is associated with depolarization line effect, whereas the width of line polarization effect is often narrower than the depolarization. Both $\Delta\lambda(I)$ and $\Delta\lambda(pol)$ are measured at full width at zero intensity (FWZI). If the line effect is detected across the absorption component of the emission line then it is considered as a McLean line effect. The line effect across the emission line is classified based on two criteria; the value of the fractional width and whether there is a flip in the polarization and PA spectra or not. If the fractional width is equal to or larger than 0.7 and there is no flip in the polarization and PA spectra across the emission line then the line effect is consistent with depolarization. On the other hand, if the fractional width is equal to or larger than 0.7 and a flip is observed in either the polarization or PA spectra then the line effect is considered to be due to intrinsic polarization. In addition, if the fractional width is smaller than 0.7 then the line effect is also consistent with polarization. In some cases two different line effects, a McLean line effect across the absorption and either depolarization or intrinsic polarization across the emission line, can be observed for the same object.

As reported before and mentioned in Section 1, a depolarization is more common in HBe stars, in particular in the early HBe stars, while in HAe stars intrinsic line polarization is the dominant line effect. To see at what spectral type the line effect switches from line polarization to depolarization, we add 9 T Tauri stars to the sample from Vink et al. (2005a) and the result is shown in Fig. 4. The figure demonstrates that the intrinsic line polarization is the dominant effect in T Tauri and late HAe stars while most early HBe

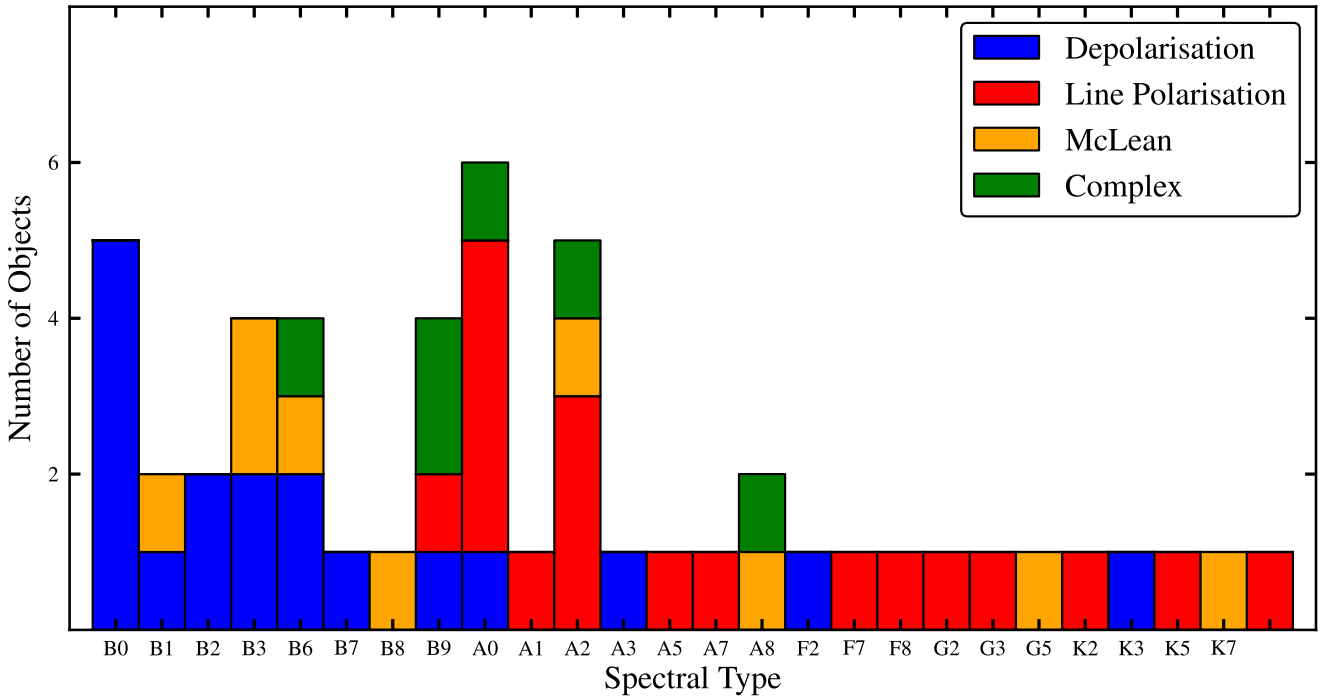

Figure 4. The figure represents the type of the observed line effect across the Hα line as a function of spectral type of a sample of the 51 HAeBe and T Tauri objects that exhibit a line effect across the polarization. Note that the B4 and B5 spectral type bins which are in the previous figure are now unpopulated, as their (only) members do not show a line effect.

stars show a depolarization. There is also a number of HBe stars with a McLean line effect. Based on the large fraction of line effects at spectral types earlier than B7 and its absence beyond that, it would appear that the line effect changes from intrinsic line polarization to depolarization around B7–B8 spectral type.

3.2.2 Line effect magnitude

Bearing in mind that the typical magnitude of the continuum polarization, and thus line effect, caused by electron scattering is expected to be 1–2 per cent (Cassinelli et al. 1987), we investigated the magnitude of the line effect for all the objects that show a clear line effect. We measured the strength of the line effects directly from the (*Q, U*) diagram. It was taken as the distance between the continuum polarization, which is visible by a cluster of points, and the line centre. The error was estimated to be typically 10 per cent. The results are tabulated in Table 2 and are also shown in Fig. 5. The polarization ranges from ∼0.3 per cent to ∼2.0 per cent with an average of ∼0.9 per cent. Only R Mon shows a magnitude of ∼10 per cent which is not expected from electron scattering close to the star and is due to observational effects as the object is spatially resolved in these observations (see the discussion in Ababakr et al. 2016). We have therefore discarded R Mon from the final results. As shown in Fig. 5, the strength of the line effect does not show any correlation with spectral type. To investigate whether the strength of the emission lines is correlated with the magnitude of the line effect, we plotted the magnitude of the latter as a function of the line peak to continuum of the Hα line (see Fig. 6). As can be seen in the figure there is only a very weak correlation between them.

3.2.3 Fractional width

Vink et al. (2002, 2005a) found that the fractional width tends to decrease towards late spectral type. We can now revise the relation by increasing the sample from 25 to 41 objects. The result is plotted in Fig. 7, the figure shows that there is a significant correlation between the fractional width and the spectral type, with a correlation coefficient, $r = -0.60$. The slope of the best fitting line between the fractional width against spectral type (counted as integers with B0 = 1, B1 = 2 etc.) is determined at the 10σ level, providing another indication that the trend is real. The intrinsic scatter around the line does prevent us from making a conclusive statement whether there is a break in the relationship or whether it is continuous however. For example, when splitting the sample into early HBe, late HBe, early HAe and late type HAe stars, we find average values of 0.90 ± 0.04, 0.79 ± 0.05, 0.74 ± 0.07, 0.61 ± 0.17, respectively (the errors are the scatter around the mean divided by the square root of the number of data points). The fractional widths measured for late HBe stars and early HAe stars are close and this might suggest they share a similar spectropolarimetric behaviour, but they themselves do not differ beyond the 2σ level from either the early Be stars or the late HAe stars. What is clear, however, is that the trend from depolarization to intrinsic polarization with the spectral type is significant. While, in addition, the early Herbig Be stars are distinctly different from the T Tauri stars for example.

4 DISCUSSION

4.1 Overall findings

In the above we have investigated various observational aspects of the linear spectropolarimetric properties of the young PMS HAeBe stars. This is the largest sample to have been studied in this manner, and this allows us to confirm that there are distinct differences between the lower mass Herbig Ae stars and the higher mass Herbig Be stars. Indeed, we find evidence that the main distinction occurs at the B7–B8 range. Furthermore, the Herbig Ae stars display a similar

behaviour as the solar mass T Tauri PMS stars. The major statistical conclusions of this exercise can be summarized as follows:

(i) The occurrence of the line effect in the entire sample is high, at 75 per cent (see e.g. Fig. 3). When considering the sample of Herbig Ae and Herbig Be stars separately, we find that the occurrence in Herbig Be stars is smaller than in Herbig Ae stars. This difference is amplified when splitting the sample in early B-type objects and the rest. The detection rate for Herbig stars of spectral type B0–B7 is 66 ± 9 per cent while that of the later type (i.e. all other) objects is 85 ± 7 per cent. Hence, this difference is close to 3σ.

(ii) The appearance of the line effect is also different as a function of spectral type. Whereas the early type objects predominately display depolarization or McLean effects, the later type objects show intrinsic line polarization. This is very clear to see from Fig. 4, where the break appears to occur around B7. Statistically, the overall change in the character of the line effect is also visible using the 'fractional width' as a quantitative handle on the nature of the line effect. Fig. 7 shows that Herbig Be stars have larger polarization widths than later type objects. The trend is significant with a slope at the 10σ level.

(iii) The strength of the line effect (in terms of per cent polarization) is of order 1 per cent and is independent of spectral type. However, there appears to be a weak trend in that stronger Hα emission lines have a slightly larger effect.

The main result of this study is that the difference between Herbig Ae and Herbig Be stars is now more robust, not only the detection rates are, statistically, shown to be different, but this 3σ effect is underpinned by the fact that the nature of the line effects is different as well. In the following, we discuss what these findings mean for the formation mechanism of low-, intermediate- and high-mass stars, and why the line effect is equally strong in these classes of object.

4.2 The origin and nature of the line effect

As discussed earlier, the intrinsic line polarization observed towards the cooler objects can be explained by compact emission such as accretion shocks on the stellar surface scattering off circumstellar material, which is found to be consistent with a disc. On the other hand, the line depolarization and McLean effect can be best explained with the presence of a small circumstellar disc. As shown in the case of classical Be stars, most of the polarization originates from a region within a few stellar radii, where the electron densities are highest. It may be surprising then that there is only a weak correlation between the magnitude of the line effect and the strength of the Hα line (or spectral type), as one could expect a stronger emission line to be associated with more ionization and more free electrons and thus a larger polarization and larger line effect.

This suggests that the detection of the line effect only depends on the geometry of the scattering agents and the geometry of the line emitting region, whereas, in the optically thin limit, the polarization itself depends on the density of the scatterers. For the depolarization line effect, the free electrons in the ionized region around the stars polarize the continuum photons while the emission photons are unpolarized. In this context, it is useful to note that, for example, Mottram et al. (2007, e.g. their Fig. 1) detected a clear line effect across the Hβ emission of HAeBe objects. For some stars, the lines are so faint that the emission does not even reach the photospheric continuum. However, in such cases, the line can still be several times stronger than the underlying photospheric emission. This is because the photospheric absorption lines' minimum can be as low

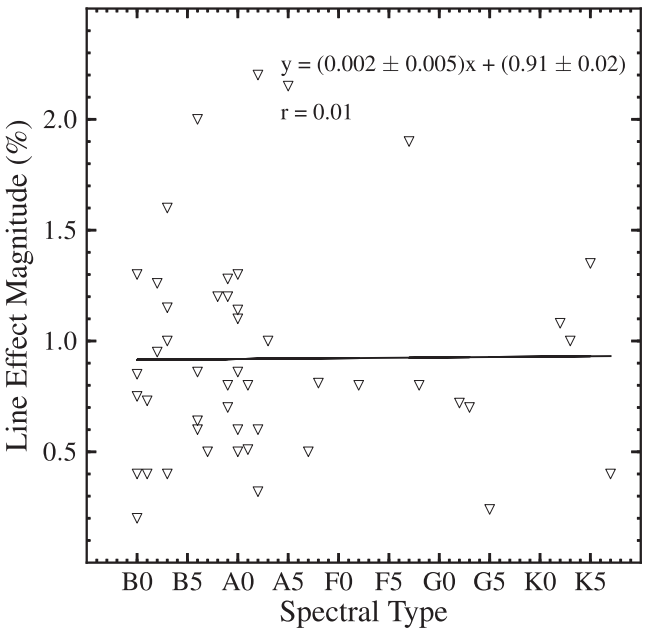

Figure 5. The figure shows the correlation between the magnitude of the observed line effect and the spectral type. The black line denotes the best-fitting straight line to the data. The best-fitting values are shown in the inset, as well as the correlation coefficient. The error on the magnitude of the line effect is below 10 per cent.

as 0.2 times the continuum level, and when the emission reaches the continuum level, it will have first filled up the underlying absorption. Most of the observed emission at these wavelengths will then be the unpolarized line emission. The maximum observable line effect, being the difference between continuum and line emission, is therefore reached already for weak lines and no, or hardly any, further changes in polarization is observed for progressively stronger lines.

In the case of the intrinsic line polarization in our objects, the line effect is due to the fact that compact line emission (such as from individual accretion hotspots or accretion funnels) scatters off circumstellar material. The cause for the ionization leading to the line emission and that responsible for the free electrons in the disc may be linked, but emission and polarization do not necessarily have to be correlated. For example the line emission arises from localized accretion hotspots and funnels in the magnetospheric accretion paradigm, while the circumstellar disc itself would be generally ionized due to the stellar photosphere and accretion luminosity. Indeed, it has been pointed out it is not yet settled whether in these situations the disc scattering material are free electrons, neutral hydrogen or dust (see e.g. Wood & Brown 1994; Vink 2015 for discussions). In any case, no trend of the strength of the line effect with line strength itself needs to be expected. In conclusion, in the above situations we can understand that the line effect strength is independent of the line strength itself. For the McLean effect, which we observe in a number of objects, this may not necessarily be the case. The number of objects with the McLean effect is rather small, eight objects, but there is no correlation between the magnitude of the line effect and the strength of the emission line. As the scattering is due to the inner regions, unrelated to the outflow or infall itself, we suspect that this also leads to a line effect independent of the line emission.

Finally, we address the question why the detection rate of the line effect in the Herbig Be stars is lower than for the Herbig Ae stars; in the case of line depolarization, the effect is a strong function

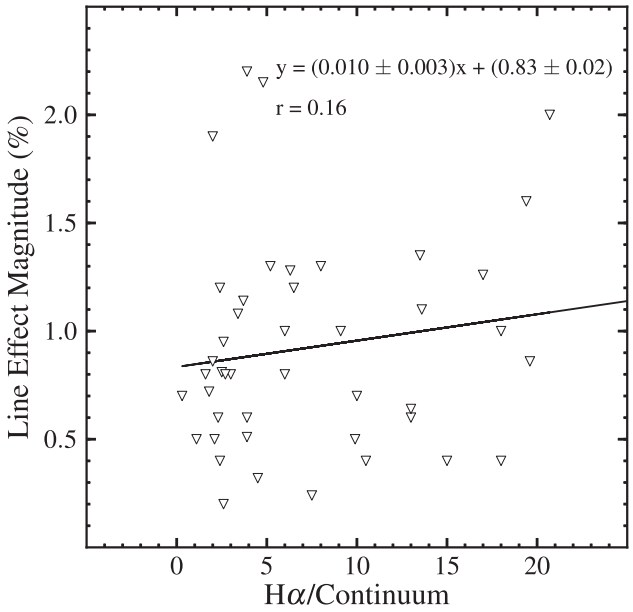

Figure 6. The correlation between the magnitude of the line effect and the strength of H α. The black line denote the best-fitting line to the data. The error on the magnitude of the line effect is below 10 per cent, and the error of the peak of H α to the continuum is less than 5 per cent.

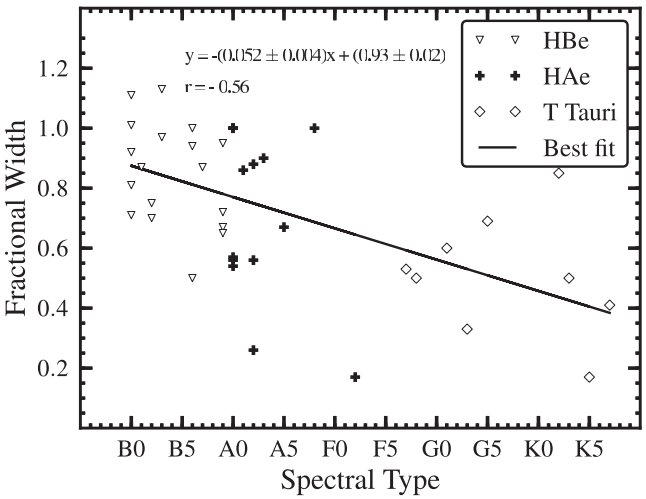

Figure 7. The fractional width of the line effect ($\Delta\lambda(pol)/\Delta\lambda(I)$) is plotted against spectral type of a sample of HAeBe and T Tauri stars. The black solid line represents the best fit of the data, the correlation coefficient $R = 0.60$, denoting a significant correlation, which is confirmed by the large, 10σ significance of the slope. The black solid circles with error bars represent the averages of early HBe, late HBe, early HAe, late HAe and T Tauri from early to late spectral type, respectively.

of inclination of the system. A larger disc inclination results in a stronger line effect (Wood, Brown & Fox 1993). When the disc is pole-on for example, the system is circular on the sky and all polarization vectors will cancel out, resulting in a net zero polarization and no difference in polarization between line and continuum. A 100 per cent detection rate will therefore not be expected at all for a sample of objects distributed at random inclinations, and the current detection rate is similar to those of classical Be stars (see e.g. Oudmaijer 2007). A difference in the case of intrinsic polarization is that polarization can be seen even at low, face-on, inclinations of the disc. This is mainly due to the fact that the compact emission is anisotropic (be it due to accretion hotspots or funnels). As a consequence only part of the disc will be illuminated. This results in a net observable polarization, and in passing we note that this also explains the higher fraction of line effects for later type stars which predominately exhibit the intrinsic polarization line effect.

4.3 On the formation of intermediate and massive stars

Our findings indicate that a break between the spectropolarimetric, and possibly accretion, properties of high- and low-mass objects occurs around the B7-B8 spectral type. This is found in both the detection statistics and, especially, the nature of the line effect. The early Herbig Be stars have a lower detection rate and show predominately the depolarization and McLean effects, indicative of circumstellar discs.

The detections are more numerous for the later B-type and A-type objects. In addition, as can be seen in Fig. 4, T Tauri stars and, especially late, HAe stars share the same H α intrinsic polarization line effect. This effect can be explained by scattering photons originating from a compact source, where the accretion take place on to the star, off the circumstellar electrons. The similarities in the spectropolarimetric properties between T Tauri stars – which are known to undergo magnetospheric accretion – and the late-type Herbig Be and Herbig Ae stars suggest this mechanism also acts on these intermediate-mass stars (cf. Vink et al. 2002 and references in the introduction).

A complication is whether HAe stars have sufficient magnetic fields to facilitate MA or not. Wade et al. (2005, 2007); Alecian et al. (2013); Hubrig et al. (2009, 2013) detected magnetic fields ($\sim$ a few hundred G) in a few HAeBe stars, mostly HAe and late HBe stars, but it is as of yet not clear whether this would be sufficient to drive accretion.

Currently, there is no well-explored theory that explains the accretion of material on to the highest mass Young Stellar Objects however. Even the most recent, sophisticated star formation models are not able to simulate the fine detail required to probe the accretion process from parsec scales via an accretion disc to the stellar surface. For example, Rosen et al. (2016) explicitly mention that the material is not followed in the inner 80 au. Given that our spectropolarimetric evidence points towards circumstellar discs that are present at very small scales, the logical, direct conclusion we can draw is that the disk is not truncated, but reaches all the way down to the stellar surface. In this situation, the so-called Boundary Layer accretion is a viable mechanism to explain the growth of massive stars. The BL is a thin annulus close to the star in which the material reduces its (Keplerian) velocity to the slow rotation of the star when it reaches the stellar surface, and it is here that kinetic energy will be dissipated. It has been explored for HAeBe stars by Blondel & Djie (2006), and the BL mechanism has also been explicitly suggested a number of times to act in Herbig Be stars (e.g. Mendigutía et al. 2011; Cauley & Johns-Krull 2015; Hartmann et al. 2016; Beltrán & de Wit 2016), however, details are yet to be worked out for the more massive Herbig Be stars.

5 CONCLUSIONS

This work presents the spectropolarimetric results of a sample of 56 HAeBe stars which is the largest linear spectropolarimetric sample of HAeBe stars that has been published to date. The main findings are as follows:

(i) Most HAeBe stars show a sign of line effect which is interpreted by the presence of a circumstellar disc. The detection rate of the line effect is 75 per cent (42/56) in the sample of 56 objects that have been observed spectropolarimetrically.

(ii) The magnitude of the line effect is of the order of 0.3–2 per cent. There is no correlation between this magnitude and spectral type. A very weak correlation is seen between the magnitude of the line effect and the strength of Hα line. We can explain this both in terms of the line depolarization and intrinsic polarization. The detection of the line effect does not rely on the strength of the emission line but on the geometry of circumstellar environment.

(iii) The Herbig Be type stars have a significantly lower detection rate than the Herbig Ae stars, with a break around spectral type B7–B8.

(iv) Most of the HBe stars' signatures are consistent with a depolarization line effect. In contrast, intrinsic line polarization is more common in HAe and T Tauri stars. It seems late HBe and early HAe stars are at the interface between the two line effects, also indicating a break in spectropolarimetric properties around B7–B8. The similarity between T Tauri, HAe stars and late Herbig Be stars suggest that the latter are forming via magnetospheric accretion.

The interface between HBe and HAe is possibly where the accretion mechanism switches from magnetospheric accretion to another process. Given the fact that the Herbig Be stars are non-magnetic and surrounded by small-scale discs, it will be interesting to consider and work out in details the Boundary Layer model as a means for the continued accretion and growth of more massive stars.

ACKNOWLEDGEMENTS

The allocation of time on the William Herschel Telescope was awarded by PATT, the United Kingdom's Panel for the Allocation of Telescope Time. KMA was supported by the UK Science and Technology Facilities Council (STFC). This research has made use of the SIMBAD data base, operated at CDS, the Centre de Données astronomiques de Strasbourg, France.

REFERENCES

Ababakr K. M., Oudmaijer R. D., Vink J. S., 2016, MNRAS, 461, 3089
Alecian E. et al., 2013, MNRAS, 429, 1001
Bailey J., 1997, Starlink User Note, 66
Beltrán M. T., de Wit W. J., 2016, A&AR, 24, 6
Blondel P. F. C., Djie H. R. E. T. A., 2006, A&A, 456, 1045
Bouvier J., Alencar S. H. P., Harries T. J., Johns-Krull C. M., Romanova M. M., 2007, in Reipurth B., Jewitt D., Keil K., eds, Protostars and Planets V. Univ. Arizona Press, Tucson, AZ, p. 479
Cassinelli J. P., Nordsieck K. H., Murison M. A., 1987, ApJ, 317, 290
Cauley P. W., Johns-Krull C. M., 2015, ApJ, 810, 5
Clarke D., McLean I. S., 1974, MNRAS, 167, 27P
Fairlamb J. R., Oudmaijer R. D., Mendigutía I., Ilee J. D., van den Ancker M. E., 2015, MNRAS, 453, 976
Fuente A., Martin-Pintado J., Bachiller R., Neri R., Palla F., 1998, A&A, 334, 253
Grady C. A. et al., 2010, ApJ, 719, 1565
Harries T. J., 1996, Starlink User Note, 204
Harrington D. M., Kuhn J. R., 2009, ApJS, 180, 138
Hartmann L., Herczeg G., Calvet N., 2016, ARA&A, 54, 135
Herbig G. H., 1960, ApJS, 4, 337
Hubrig S. et al., 2009, A&A, 502, 283
Hubrig S., Ilyin I., Schöller M., Lo Curto G., 2013, Astron. Nachr., 334, 1093
Ilee J. D., Fairlamb J., Oudmaijer R. D., Mendigutía I., van den Ancker M. E., Kraus S., Wheelwright H. E., 2014, MNRAS, 445, 3723
Jaschek C., Jaschek M., 1990, The Classification of Stars. Cambridge Univ. Press, Cambridge
Kraus S., 2015, Ap&SS, 357, 97
Kraus S., Preibisch T., Ohnaka K., 2008, ApJ, 676, 490
Kurosawa R. et al., 2016, MNRAS, 457, 2236
McLean I. S., 1979, MNRAS, 186, 265
Mendigutía I., Calvet N., Montesinos B., Mora A., Muzerolle J., Eiroa C., Oudmaijer R. D., Merín B., 2011, A&A, 535, A99
Mendigutía I., de Wit W. J., Oudmaijer R. D., Fairlamb J. R., Carciofi A. C., Ilee J. D., Vieira R. G., 2015, MNRAS, 453, 2126
Mendigutía I., Oudmaijer R. D., Mourard D., Muzerolle J., 2017, MNRAS, 464, 1984
Mottram J. C., Vink J. S., Oudmaijer R. D., Patel M., 2007, MNRAS, 377, 1363
Muzerolle J., D'Alessio P., Calvet N., Hartmann L., 2004, ApJ, 617, 406
Oudmaijer R. D., 2007, in Hartquist T. W., Falle S. A. E. G., Pittard J. M., eds, Diffuse Matter From Star Forming Regions to Active Galaxies. Springer-Verlag, Berlin, p. 83
Oudmaijer R. D., 2017, in Miroshnichenko A., Zharikov S., Korčáková D., Wolf M., eds, ASP Conf. Ser. Vol. 508, The B[e] Phenomenon: Forty Years of Studies. Astron. Soc. Pac., San Francisco, p. 175
Oudmaijer R. D., Drew J. E., 1999, MNRAS, 305, 166
Patel P., Sigut T. A. A., Landstreet J. D., 2017, ApJ, 836, 214
Poeckert R., Marlborough J. M., 1976, ApJ, 206, 182
Quirrenbach A. et al., 1997, ApJ, 479, 477
Rosen A. L., Krumholz M. R., McKee C. F., Klein R. I., 2016, MNRAS, 463, 2553
Schaifers K., Voigt H. H., Landolt H., Boernstein R., Hellwege K. H., 1982, Astronomy and Astrophysics. B: Stars and Star Clusters. Springer-Verlag, Berlin
Schöller M. et al., 2016, A&A, 592, A50
Testi L., Palla F., Natta A., 1999, A&A, 342, 515
Thé P. S., de Winter D., Pérez M. R., 1994, A&AS, 104, 315
Tody D., 1993, in Hanisch R. J., Brissenden R. J. V., Barnes J., eds, ASP Conf. Ser. Vol. 52, Astronomical Data Analysis Software and Systems II. Astron. Soc. Pac., San Francisco, p. 173
Trammell S. R., Dinerstein H. L., Goodrich R. W., 1994, AJ, 108, 984
Vieira S. L. A., Corradi W. J. B., Alencar S. H. P., Mendes L. T. S., Torres C. A. O., Quast G. R., Guimarães M. M., da Silva L., 2003, AJ, 126, 2971
Vink J. S., 2015, Ap&SS, 357, 98
Vink J. S., Drew J. E., Harries T. J., Oudmaijer R. D., 2002, MNRAS, 337, 356
Vink J. S., Drew J. E., Harries T. J., Oudmaijer R. D., Unruh Y. C., 2003, A&A, 406, 703
Vink J. S., Drew J. E., Harries T. J., Oudmaijer R. D., Unruh Y., 2005a, MNRAS, 359, 1049
Vink J. S., Harries T. J., Drew J. E., 2005b, A&A, 430, 213
Wade G. A. et al., 2005, A&A, 442, L31
Wade G. A., Bagnulo S., Drouin D., Landstreet J. D., Monin D., 2007, MNRAS, 376, 1145
Wheelwright H. E., Vink J. S., Oudmaijer R. D., Drew J. E., 2011, A&A, 532, A28
Wood K., Brown J. C., 1994, A&A, 291, 202
Wood K., Brown J. C., Fox G. K., 1993, A&A, 271, 492

APPENDIX A: OBSERVED SPECTROPOLARIMETRIC SIGNATURES

Here, we present the spectropolarimetric results across Hα for the new observations.

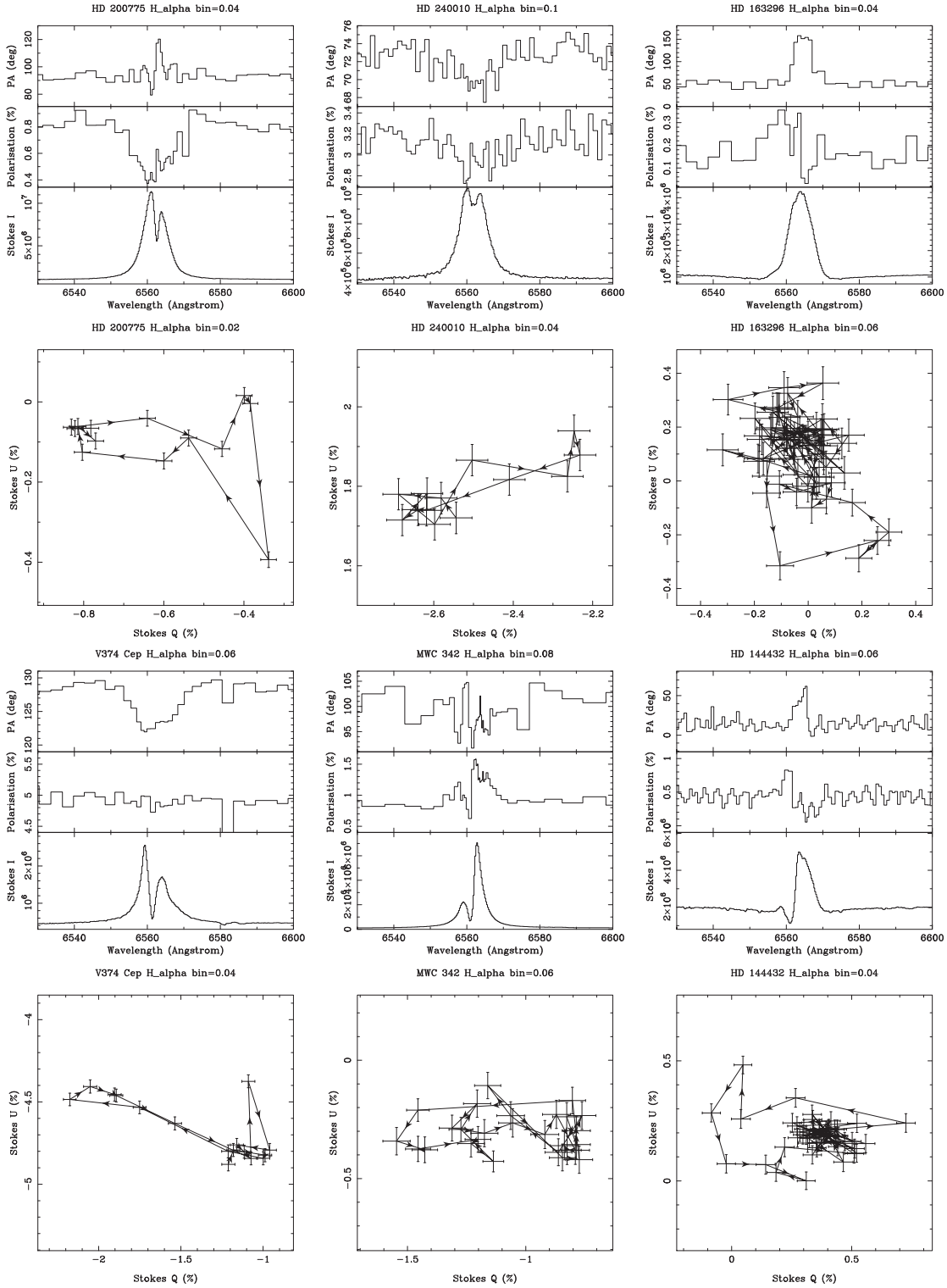

Figure A1. Hα spectropolarimetry of the stars. The data are presented as a combination of triplots (top) and (*Q, U)* diagrams (bottom). In the triplot polarization spectra, the Stokes intensity (I) is shown in the bottom panel, polarization (per cent) in the centre, while the position angle (PA) is shown in the upper panel. The *Q* and *U* Stokes parameters are plotted against each other below each triplot. The data are rebinned to a constant error in polarization, which is indicated at the top of each plot. The arrows in the (*Q, U)* diagrams indicate the polarization moves in and out of the line effect from blue to red wavelengths.

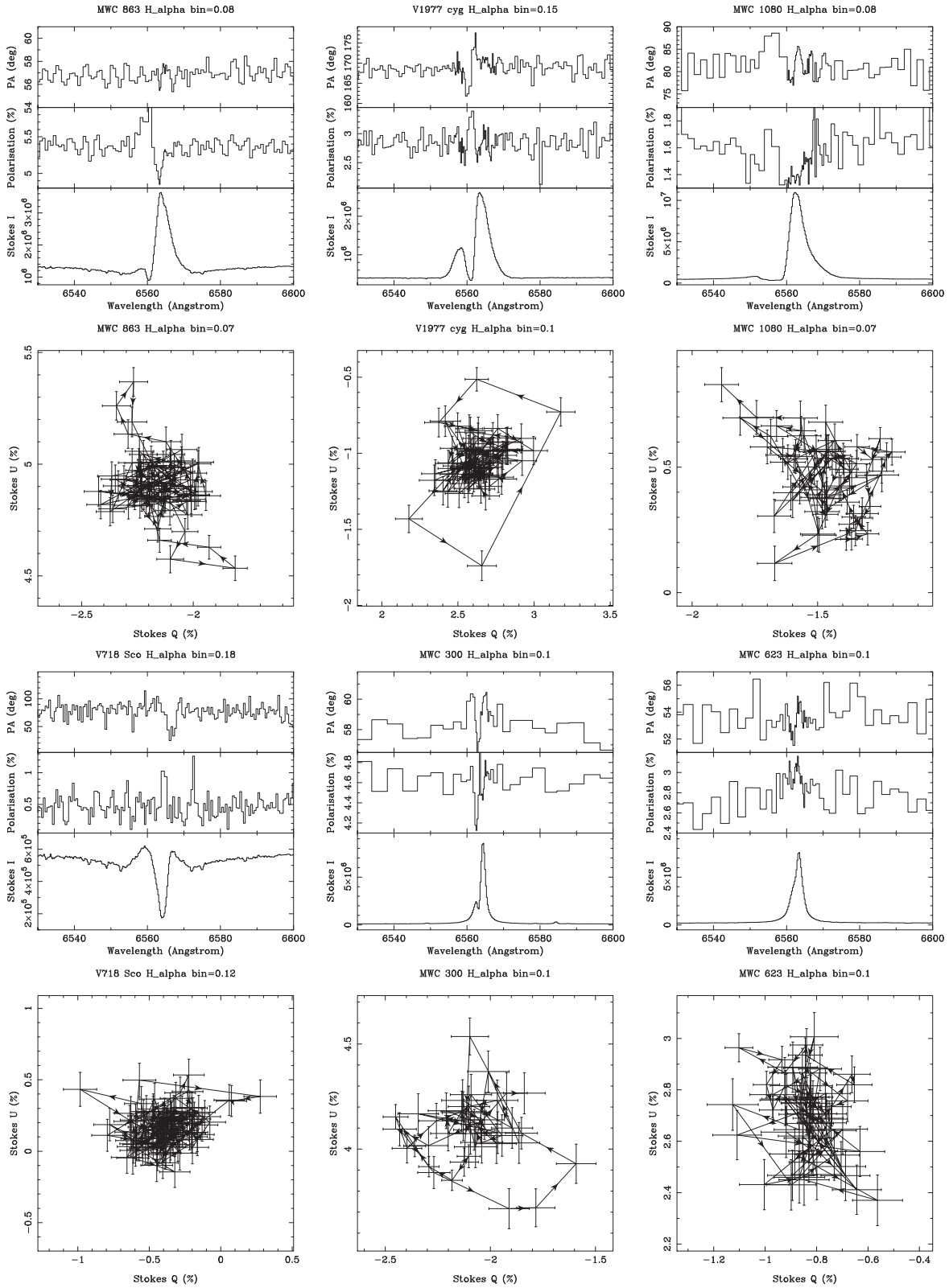

Figure A1 – *continued*

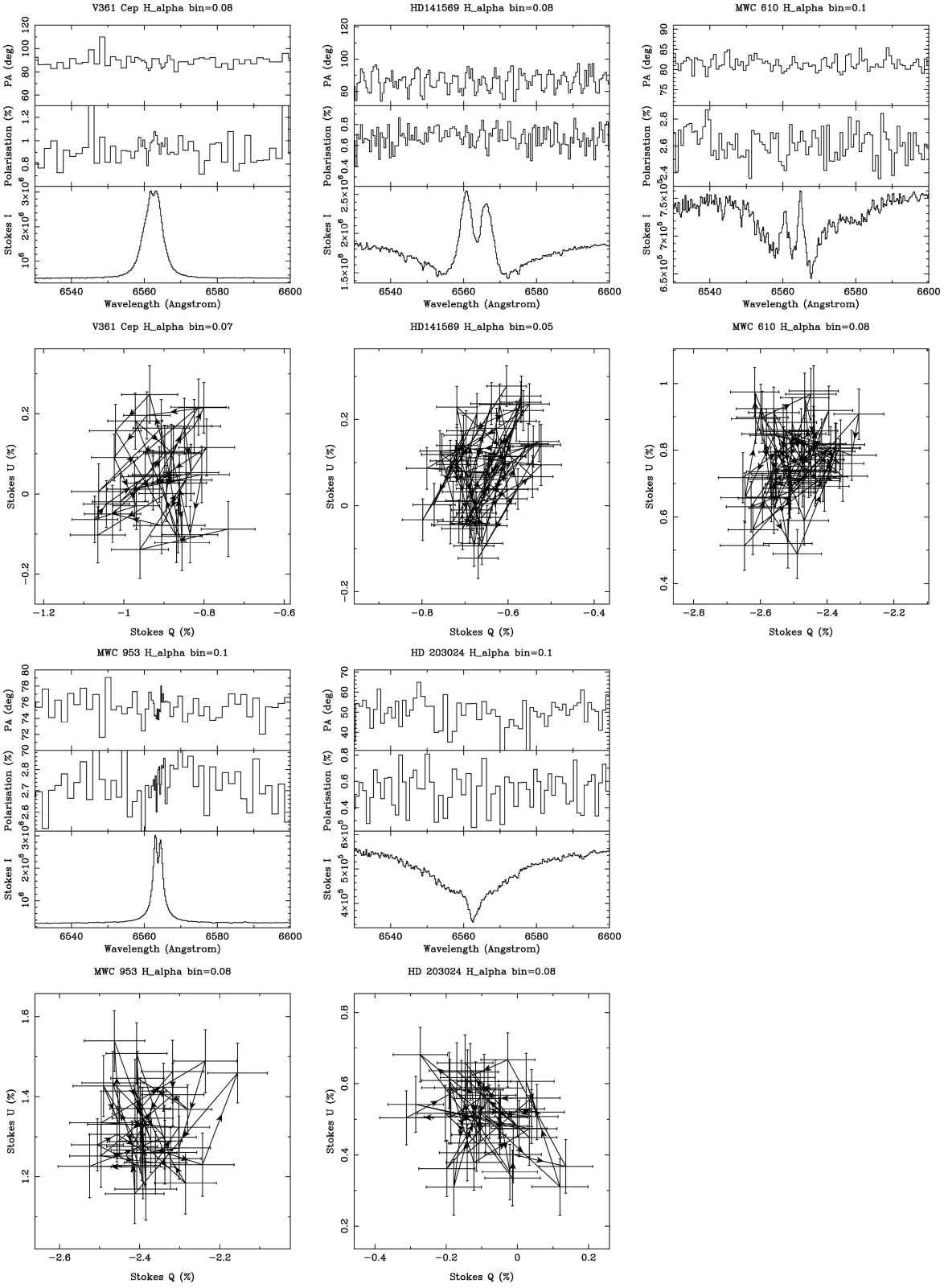

Figure A1 – *continued*

This paper has been typeset from a TEX/LATEX file prepared by the author.